Versatile protein-templated TiO_2 nanocomposite for energy storage and catalytic applications

*Daily Rodríguez-Padrón,[a]‡ Alain R. Puente-Santiago,[a]‡ Fernando Luna-Lama,[b] Álvaro Caballero,[b] Mario J. Muñoz-Batista,[a] *and Rafael Luque[a,c]**

[a] Departamento de Química Orgánica, Instituto de Química Fina y Nanoquímica, Universidad de Córdoba, Campus de Rabanales, Edificio Marie Curie (C-3), Ctra Nnal IV-A, Km 396, E14014, Cordoba, España. * M.J.M-B.: qo2mubam@uco.es, R.L.: rafael.luque@uco.es

[b] Departamento de Química Inorgánica e Ingeniería Química, Instituto de Química Fina y Nanoquímica, Universidad de Córdoba, Campus de Rabanales, Edificio Marie Curie (C-3), Ctra Nnal IV-A, Km 396, E14014, Cordoba, España.

[c]Peoples Friendship University of Russia (RUDN University), 6 Miklukho-Maklaya str., 117198, Moscow, Russia.

‡These authors contributed equally to the work.

Abstract

A protein-templated titania nanocomposite (PT-TiO_2) was successfully synthesized by a water-free mechanochemical approach. A biomass valorization strategy was developed by employing egg white from expired eggs to control the morphology and textural features of the prepared titania. A remarkable enhancement of the surface area was achieved, in comparison with the synthesis of the material in absence of the biomass-derived template. Several techniques, such as SEM-mapping and CNHS analysis, supported the presence of carbon, nitrogen and sulfur residues in the obtained composite. Catalytic performance of PT-TiO_2 was explored in the oxidation of diphenyl sulfide, displaying promising results in terms of conversion, selectivity and stability. The effect of the oxidant agent was additionally investigated by using hydrogen peroxide, urea hydrogen peroxide, oxygen and t-butyl- hydroperoxide. On the other hand, PT-TiO_2 nanocomposite was successfully proved as anodic material for LIBs delivering a reversible capacity of 107 mAh g^{-1} at 0.1 C with an excellent coulombic efficiency of 100% from the second cycle. In addition, the as-synthesized material showed significant capacity retention values of 76% among the second cycle and 100th cycle. PT-TiO_2 sample resulted to be a versatile material with potential catalytic and energy storage applications.

Keywords: White egg, titania, biomass valorization, LIBs, microwave assisted reaction, diphenyl sulfide oxidation.

Introduction

Development of new systems to produce sustainable energy and its efficient use are two of the main problems of modern-day society. It is well-known that energy vectors generated from traditional fuel-fossil sources and processes are basically responsible for problems of climate change and, as a response, the development of greener and highly efficient technologies, such as solar cells, lithium-ion batteries (LIBs) or production of new energy vectors (e.i. H_2) are presented as a potential alternative.[1,2] How we use the energy in the wide range of application available has equal relevance in the complicated current energy context. In particular, chemical industry is being one of the higher energy consumers around the world which makes the development of increasingly energy processes a key challenge of modern society. To solve the mentioned drawbacks, non-traditional energy sources for chemical applications have been gaining more interest in both laboratories and industrial scales. In this regard, the use of sustainable materials as 1) anode component for lithium-ion batteries (LIBs) with high and stable capacities and as 2) catalyst for microwave-assisted reactions has received considerable attention.[3–5]

Field of catalysis is very dependent on energy, requiring in many cases high energy consumption operating conditions such as high temperatures and pressures. For instance, natural or artificial light-assisted as well as sonication and microwave reactors have boosted energy efficiency in several catalytic processes, from new synthetic protocols to reactions.[6–10] Among a large variety of materials studied for catalytic applications, TiO_2-based compounds are presented as a promising alternative. Additionally, they have even been used as effective anode materials towards the generation of high-performance LIBs.[11,12] In fact, some reviews highlight TiO_2 as the most studied transition-metal oxide and one of the most investigated compounds in materials science.[13,14] Such versatility has produced an increase in scientific activity in this direction. From a structural point

of view, relatively high surface areas in addition to small crystal sizes can be beneficial to many TiO_2-based materials and its application, as it improves the interaction between the samples and media.[7,13–16] There are several contributions in which structure and morphology properties of TiO_2 have been analyzed as a function of the synthetic protocol.[7,17] In this regard, although methods such as sol-gel, microemulsion, hydrothermal and microwave-assisted have shown several advantages and have produced an extended number of applicable materials,[18–21] also possess inherent disadvantages. Some of them with negative environmental effects regarding to high temperatures and the use of high levels of solvents and reagents. In this sense, biomass-derived templates have emerged as a simple and outstanding approach to produce TiO_2 materials minimizing time, chemicals, external water and waste.[22] Food residues constitute a significant part of non-used biomass materials. In fact, it is a problem extensively addressed by U.S. Environmental Protection Agency.[23] The aforementioned template methods could be a profitable outlet for both food residues and out of date food. Banana and orange peel, chicken egg and coffee waste grounds can be mentioned as representative examples, which have provided outstanding results as bio-template.[24–27] In addition, with proper control of the calcination process, it is possible to maintain in the structure beneficial entities from the bio-template as is the case of biomass-derived nitrogen-doped carbon-oxides materials. Besides, biomass residues confers high oxygen functionalities to the resulted carbons, which can act as anchoring sites for further metal deposition.[4]

In this contribution, we addressed an easy and environmental friendly synthesis of a TiO_2-based composite using white egg by a template methodology for catalytic and energy storage applications. The suitable balances of all properties allow obtaining a good reversible capacity (similar to other TiO_2 based electrode materials) as well as highly selective catalyst for the

oxidation of diphenil sulfide to the corresponding sulfoxide. P25 TiO_2 is also reported as a commercial reference for both applications. Finally, a complete physico-chemical characterization of the as synthesized material attempts to correlate the results with a multitechnique characterization approach based on data obtained from XRD, XPS, SEM-EDX as well as N_2 physisorption measurements.

Experimental

Synthesis of protein-templated-TiO_2 (PT-TiO_2)

A water-free mechanochemical assisted protocol was employed for the synthesis of PT-TiO_2 sample (Scheme 1). Firstly, a 1:2 (wt.) metal precursor (titanium isopropoxide)/template (egg white from expired eggs: 40 days) ratio was mixed in a 125 mL reaction chamber and mechanochemically treated in a Retsch PM100 ball mill at 350 rpm for 10 min, employing eighteen 10 mm stainless steel balls. In a second step, the obtained composite material was oven-dried at 100 °C for 24 h, and finally calcined at 500 °C for 2h.

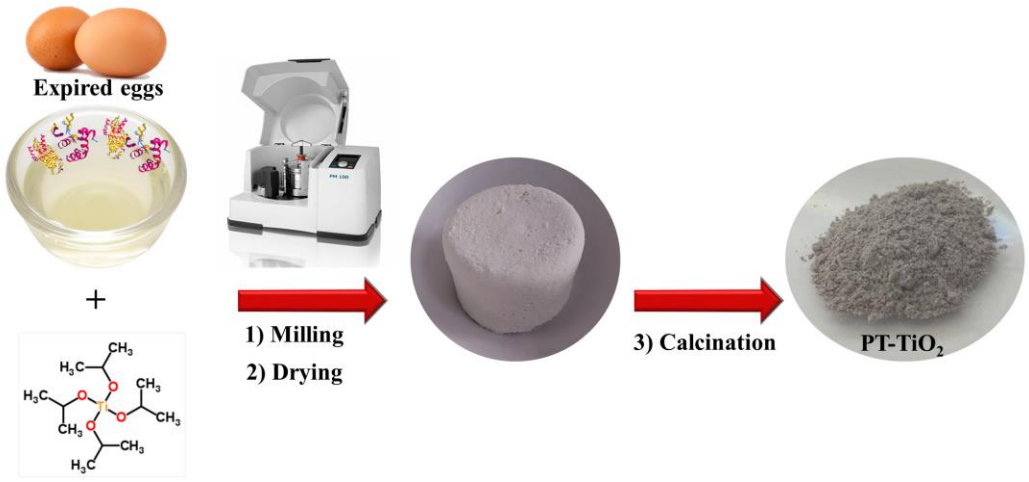

Scheme 1. Schematic representation of the synthetic protocol of PT-TiO_2 material.

Chemical analysis and textural characterization

The prepared PT-TiO_2 material was characterized by several techniques, including X-ray diffraction (XRD), X-Ray Photoelectron Spectroscopy (XPS), Thermogravimetric analysis (TGA), N_2 physisorption, Scanning Electronic Microscopy, Transmission Electronic Microscopy and CNHS measurements.

XRD analysis of PT-TiO_2 sample was accomplished in a Diffractometer (D8 Advanced Bruker AXS), employing a Lynxeye detector in a 10°-70° 2θ scan range. Results interpretation was performed helped by the Bruker Diffrac-plus EVA software and supported by the Powder Diffraction File (PDF) database of the International Centre for Diffraction Data (ICDD).

N_2 physisorption analysis was accomplished at the temperature of liquid nitrogen (77 K) in a Micromeritics ASAP 2000 instrument. Prior to analysis, TiO_2 reference and PT-TiO_2 sample were degassed for 24 h under vacuum ($p<10^{-2}$ Pa). The weight of both materials ranged between 0.15-0.20 g. BET analysis, in a $0.05<P_0<0.30$ range, was employed for determining the surface areas of the prepared materials. TGA measurements were accomplished on a Setaram Setsys 12 TGA thermobalance. The sample was heated from 30 to 800 C, under air atmosphere (50 mL min^{-1}) at a rate of 10 °C min^{-1}.

The FEI Tecnai G2 system equipped with a CCD ("charge coupling device") camera was used in order to record TEM images of the synthesized materials. PT-TiO_2 sample was previously suspended in ethanol and subsequently deposited on a copper grid. SEM-mapping measurements were performed in a JEOL JSM-6490 LV microscope.

XPS experiments were carried out in an ultrahigh vacuum (UHV) multipurpose surface analysis system SpecsTM, equipped with the Phoibos 150-MCD energy detector. The measurements were carried out at pressures $<10^{-10}$ mbar, employing a X-ray source in a "stop and go" mode. XPS CASA program was used for analysis the obtained data.

Preparation of the electrodes and cells

The as-synthesized PT-TiO_2 material was mechanically mixed with PVDF polymer and a super conductive carbon black in a 1-methyl-2-pyrrolidinone solution (NMP) to (80:10:10) to obtain the anode material. Firstly, the resulting solution was deposited through the “doctor-blade” approach onto a Cu thin foil and secondly tiny disks of 13 mm were cut and were dried at 50 °C in vacuum conditions to fabricate anode electrodes, following previous work.[27]

Electrochemical characterization

Electrochemical characterization was performed using a reported setup.[27] Cyclic voltammetry (CV) measurements were acquired in a potential range of 0–3 V. Charge-discharge curves were carried out at 0.1A at a current rate of 0.1 A g^{-1} (approximate to 0.3C) and rate capability behaviour was tested varying current density from 33.5 to 670 mA g^{-1}.

Results and discussion

The preparation of the protein-templated TiO_2 nanocomposite (PT-TiO_2) was performed using egg white from expired eggs and titanium isopropoxide as metal precursor, by a solvent-free mechanochemical strategy. Apart from its noticeable versatility, reproducibility and simplicity, the application of mechanochemistry as a synthetic procedure possess a marked sustainable character, since it avoids the employment of solvents and additional reagents. In this work, egg white was

employed as a template in order to tune the morphological properties of the obtained TiO_2. Titanium isopropoxide together with the aforementioned template gave rise to a composite material by physical and/or chemical adherence. Besides the effect in the morphological properties, the presence of water from egg white also allows the hydrolysis of the titanium precursor, resulting in the formation of titanium hydroxide. The latest compound was calcined at 500 ºC, with the consequent formation of a nanostructured titanium oxide composite.

Structural characterization of the TiO_2-based nanocomposite.

The synthesized protein-templated TiO_2 nanocomposite was fully characterized by a multi-technique approach, including X-ray Diffraction (XRD), N_2-physisorption, Thermogravimetric analysis (TGA), Transmission Electronic Microscopy, Scanning Electronic Microscopy, CHNS measurements and X-ray Photoelectronic Spectroscopy (XPS). For comparison, a TiO_2 material was additionally prepared by a similar protocol in absence of the template. Basic characterization of such TiO_2 reference was performed by XRD and N_2-physisorption.

Crystal structure and arrangement of PT-TiO_2 and TiO_2 reference were evaluated by XRD analysis. XRD pattern of TiO_2 reference displayed a highly crystalline structure with the presence of several peaks at 25.4º, 37.0º, 37.9º, 38.5º, 48.1º, 54.0º, 55.1º and 62.8º, which can be attributed to (101), (103), (004), (112), (200), (105), (201) and (204) diffraction planes, respectively.[28] Although the peaks in the XRD pattern of PT-TiO_2 sample exhibited a reduced intensity, (Figure 1A) associated with a lower crystallinity, in comparison with the TiO_2 reference, both samples presented the same crystalline phase, namely anatase. This result could be attributed most likely to the mediation of the template in the synthetic process.

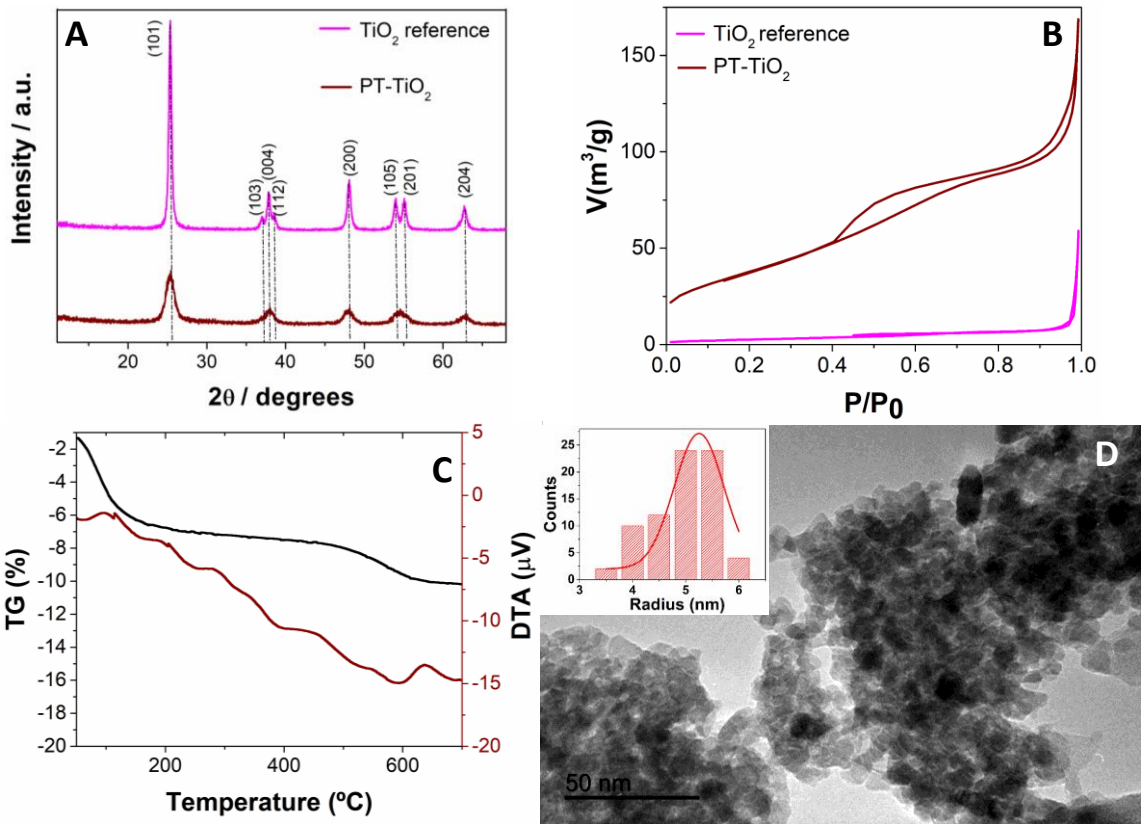

Figure 1. (A) XRD patterns and (B) N_2 absorption-desorption isotherms of PT-TiO_2 and TiO_2 reference, (C) TG and DTA analyses of PT-TiO_2, (D) TEM image of PT-TiO_2 (Inset: Particle size distribution).

Textural properties of both samples, PT-TiO_2 and TiO_2 reference, were investigated by N_2 adsorption-desorption measurements. A remarkable enhancement of the morphological features was observed by using egg white as template, as shown in Figure 1B. N_2 adsorption-desorption isotherms resulted to be type III and IV for TiO_2 reference and PT-TiO_2, respectively. Such result confirmed the mesoporous structure and the improved textural properties of the PT-TiO_2 in comparison with the material prepared in absence of the template. An outstanding surface area of 139 m^2g^{-1} was found for the PT-TiO_2 material, while TiO_2 reference displayed just a surface area of 10 m^2g^{-1} (Table 1). The superficial area of the composite, which is an important property for

the studied application, is competitive in comparison with other synthetic methods such as sol-gel, micro-emulsion or hydrothermal in which the presence of external water and other solvents are required.[18–21] These results clearly confirmed the crucial role of the template in the controllable tuning of the material textural characteristics. Thermal stability of the prepared PT-TiO_2 was studied by TGA measurements (Figure 1C). A first weight loss was found at 100 ºC, related to the presence of water (unbounded/physisorbed). Afterwards, a progressive and slow weight loss of 10 % was observed from 200 to 700 ºC (broad endothermic–DTA signal). This result can be attributed to the non-oxidative decomposition of organic residues in the PT-TiO_2.[27]

Table 1. Textural properties of the PT-TiO_2 and TiO_2 reference.

Material	**S_{BET} (m^2 g^{-1})**	**V_{BJH} (cm^3 g^{-1})**	**D_{BJH} (nm)**
PT-TiO_2	139	0.07	20.2
TiO_2 reference	10	0.25	5.7

Figure 1D exhibit TEM micrograph of the PT-TiO_2 sample, which revealed a homogenous distribution of quasi-spherical nanoparticles with a mean radius of 5.2 nm. In addition, the morphology of the prepared material was evaluated by SEM analysis, which was in accordance with the nanostructured architecture observed by TEM. SEM-mapping results suggested the presence of Ti and O, as well as C, N and S, most likely due to the presence of protein residues in the obtained nanocomposite (Figure 2). Such results were corroborated by CNHS measurements, which showed 1.0 %, 1.3% and 0.4% of N, C and S, respectively.

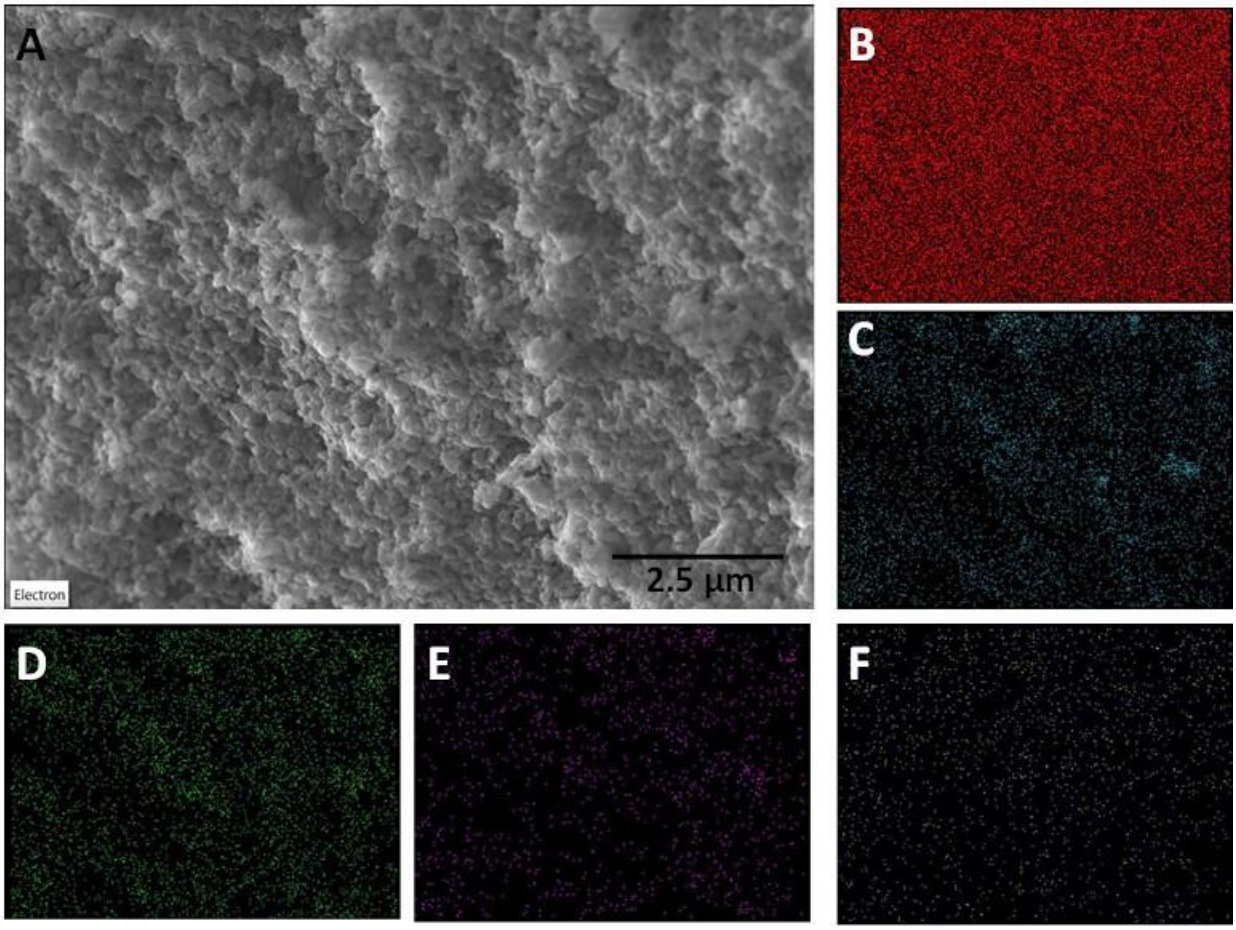

Figure 2. (A) SEM micrograph of PT-TiO_2 sample. SEM-mapping images of PT-TiO_2 sample for (B) Ti, (C) O, (D) C, (E) N and (F) S.

XPS analysis of the nano-composite was carried out to provide information related to the minor carbon, nitrogen, and sulphur species, as well as titanium and oxygen components. Figure 3A displays the C1s region. The main contribution can be related to spurious entities generated during the calcination process, although can also be associated to residual aliphatic C−H bonds of the albumin (284.6 eV).[29] The other two contributions can exclusively ascribable to different C-N structural moieties (286.2 and 287.9 eV), generated during heating treatment due to the denaturalization process of the protein.[30] These two chemical moieties (399.5 and 397.3 eV) also

contribute to the N1s XPS region (Figure 3B). For S2p the fitting takes into two contributions, S2p3/2 and S2p1/2 (153.8 and 152.2 eV, respectively), resulting from the sulphur atoms coming from the protein molecules.[25] Ti2p core level spectra shows typical contribution of titania. The corresponding Ti 2p3/2 and Ti 2p1/2 peaks are located at 458.6 eV and 463.8 eV, respectively and correspond to Ti(IV).[31] Finally, the analysis of O1s XPS was fitted into two components indicating the presence of the two types of oxygen expected in the sample. The main peak at 529.3 eV can be assigned to the oxygen lattice ions of the anatase network (Ti-O-Ti) and the contribution situated at 531.5 eV to the C-O. [31,32]

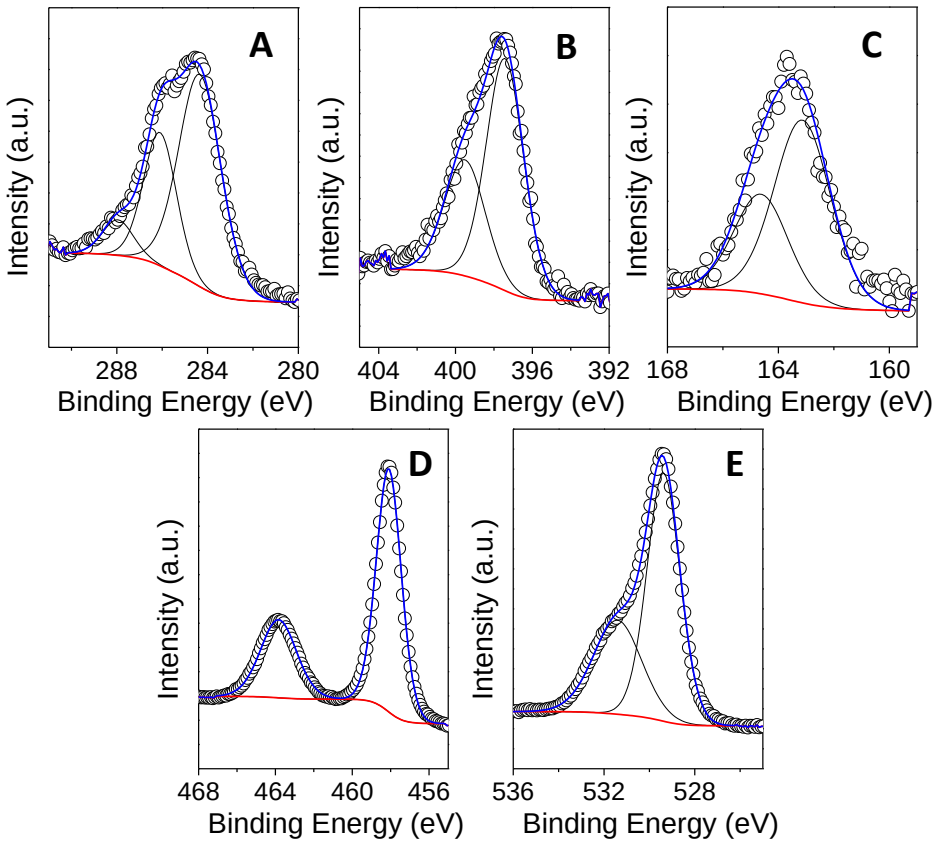

Figure 3. XPS deconvoluted spectra of PT-TiO_2 sample for (A) C1s, (B) N1s, (C) S2p, (D) Ti2p and (E) O1s.

Catalytic performance of PC-TiO_2 nanocomposite

The catalytic performance of PT-TiO_2 sample was evaluated in the microwave-assisted oxidation of diphenyl sulfide to the corresponding sulfoxide and sulfone (Scheme 2). The microwave irradiation was employed in order to decrease the reaction times, favoring as well the efficiency of the catalytic process, in terms of conversion. Sulfoxidation has been usually hindered by problems related to the selectivity of the reaction, being particularly interesting the selective production of sulfoxide molecules (alkyl, aryl and benzyl derivatives) with potential applicability in the pharmaceutical industry. The selectivity of such kind of reactions will partially depend on the employed catalytic system. Specially, the use of heterogeneous catalysts possesses intrinsic advantages related to their easy recovery and reuse. Several contributions have reported sulfoxidation reactions in the presence of heterogeneous catalyst such as transition metal functionalized graphene oxide, ionic liquid complexes, transition-metal oxide clusters, tungsten (VI) organic complexes and carbon supported polyoxometalates. Remarkably, the prepared PT-TiO_2 material is advantageous, with respect to the aforementioned systems, due to its simple structure and facile preparation methodology.

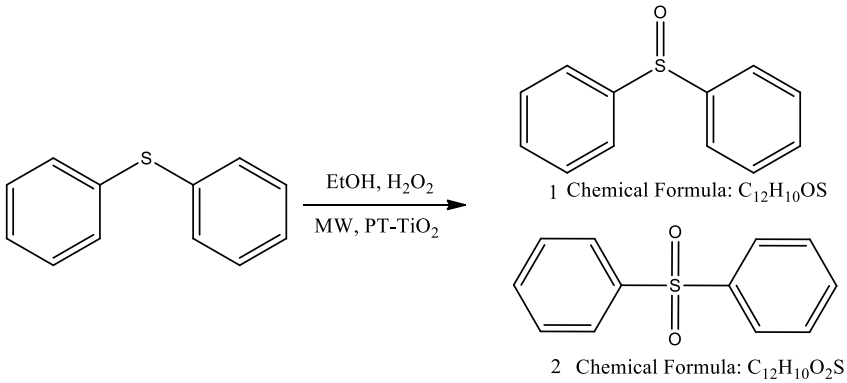

Scheme 2. Schematic representation of the diphenyl sulfide microwave-assisted oxidation.

Blank measurements were performed in order to confirm the essential role of the catalytic system in the reaction progress. Such analysis revealed that in absence of catalyst the reaction just displayed a 10% of conversion. In turn, by using the prepared PT-TiO_2 catalytic material, the reaction achieved a 90% of conversion (Figure 4A). P25 titania was, as well, employed in the oxidation of diphenyl sulfide, in order to compare the prepared material with a commercial reference. Both materials displayed comparable results in terms of conversion, however a critical change in selectivity was observed (Figure 4B). The employment of P25 material, give rise to the complete oxidation of diphenyl sulfide to sulfone, with a selectivity to this product higher that 95%. On the other hand, the use of PT-TiO_2 allows the controllable oxidation of sulfide group to the corresponding sulfoxide, with a selectivity to this product of 90%. Such result could be understood attending the different crystallinity of both samples and to the presence of carbon species on the PT-TiO_2 surface. A decrease in crystallinity could be associated with a decrease in selectivity to the full oxidation product, most likely due to the reduction of active sites that promote, in this case, the complete oxidation of sulfide to form the sulfone product. As aforementioned, reported conversion were obtained after 1 h of reaction, faster than similar experiments carried out under typical operating conditions (temperature and oxidant agent).[33,34] Note that carbon balance was achieved above 97% in all catalytic tests, and thus only rather minor products are not shown.

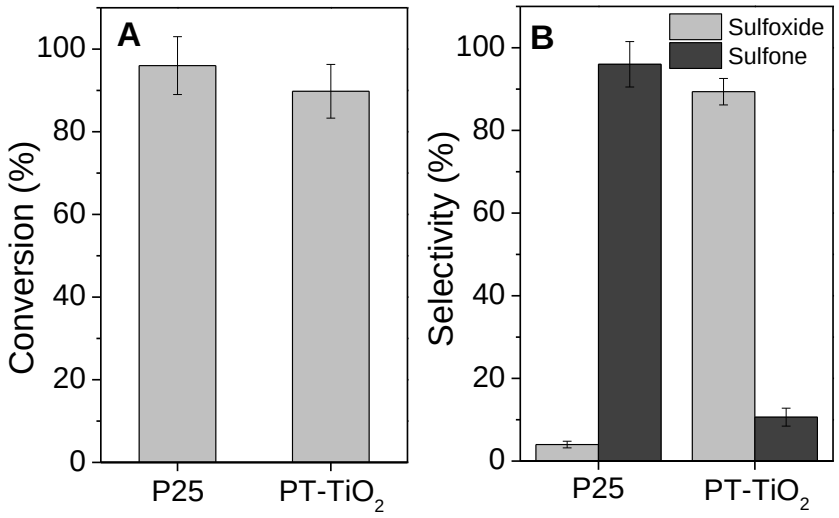

Figure 4. Catalytic performance of PT-TiO_2 and TiO_2 P25, in terms of (A) conversion and (B) selectivity.

As shown in Figure 5, the influence of the oxidant agent was investigated by comparing the catalytic performance employing hydrogen peroxide, urea hydrogen peroxide (U-H_2O_2), oxygen and *t*-butyl- hydroperoxide (*t*-B-H_2O_2). The use of hydrogen peroxide presented the best catalytic performance in terms of balance between conversion (90 %) and selectivity (90 %). Although, selectivity to diphenyl sulfide increase by using U-H_2O_2 (S=94 %), O_2 (S=94 %) and *t*-B-H_2O_2 (S=96 %), the conversion decrease to 53 %, 5 % and 15 % conversion, respectively, support the use of hydrogen peroxide as the optimum oxidant agent.

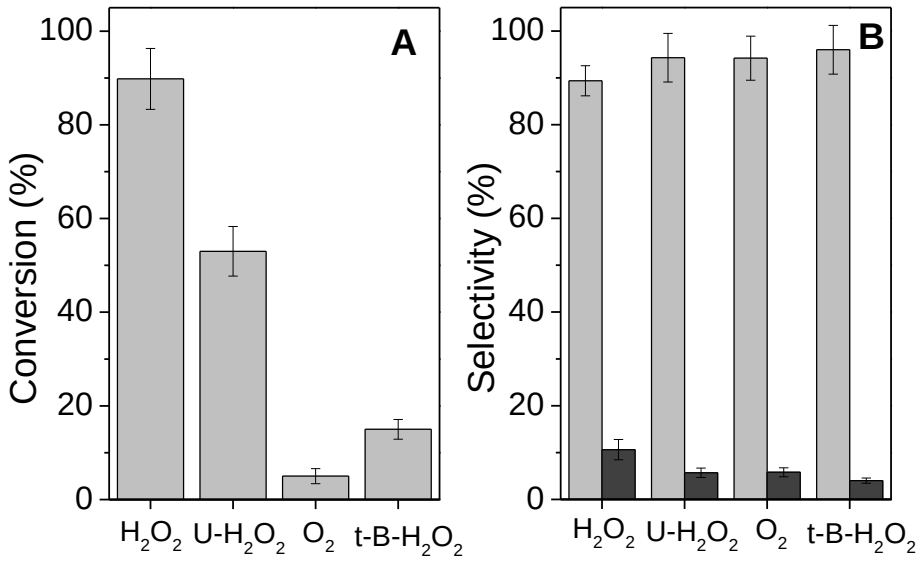

Figure 5. Catalytic performance of PT-TiO_2 employing different oxidant agents, in terms of (A) conversion and (B) selectivity.

Reusability studies were carried out in order to determine the stability of the material (Figure 6). After the first use, the catalyst was recovered, washed and reused in the reaction under identical operating conditions. Such process was repeated five times, revealing that the catalytic system remained stable, showing an 86 % conversion after the fifth use, with no considerable change in selectivity.

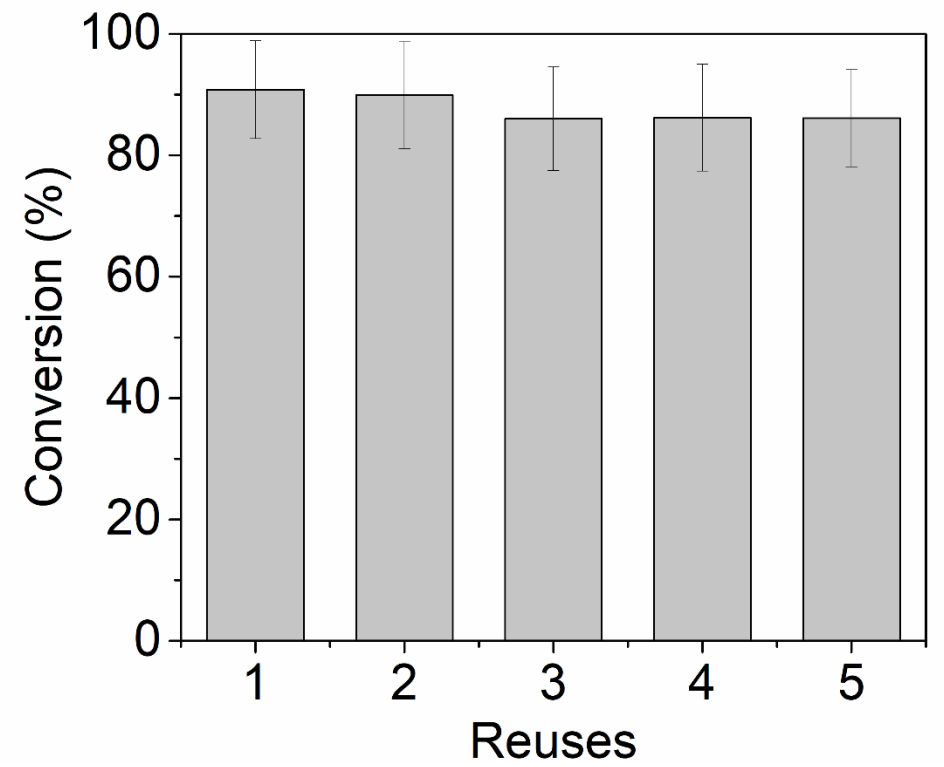

Figure 6. Reusability study of PT-TiO_2 nanocomposite.

Electrochemical characterization of PC-TiO_2 nanocomposite

The electrochemical performance of the PT-TiO_2 nanocomposite was explored as anode for lithium ion batteries and compared with the commercial TiO_2 material (P25). Figure 7A and 7B show the typical cyclic voltammogram (CV) curves of the PT-TiO_2 and P25 anode materials measured in the potential window of 1-3V at a sweep rate of 0.1 mV/s. The voltammograms of the mentioned anode materials display two pair of well-defined and stable peaks at 1.72 and 2.01V (vs Li^+/Li) indicating the lithium insertion/extraction processes in the crystalline anatase structure. Importantly, the higher intensities of the cathodic and anodic redox peaks of the PT-TiO_2 hybrid nanostructures regarding to the commercial TiO_2 structures represent a clear evidence of its enhanced electrochemical activity. The evolution of the cathodic potential peak (E_c) and anodic potential peak (E_a) for both anode materials are shown in Figure 7C and 7D. It can be observed

that at faster scan rates, in comparison with P25 anode electrodes, the potential peak separation as well as the peak shape of the PT-TiO_2 nanocomposite is closer to the initial voltammogram measured at a scan rate of 0.1 mV/s. Additionally, the PT-TiO_2 peak intensities surpassed around ten times the signal intensities of the commercial sample. The aforementioned behaviour revealed the higher reversibility of the TiO_2 nanocomposite material and supported its better electrochemical efficiency as an anode material in lithium half-cells.[32]

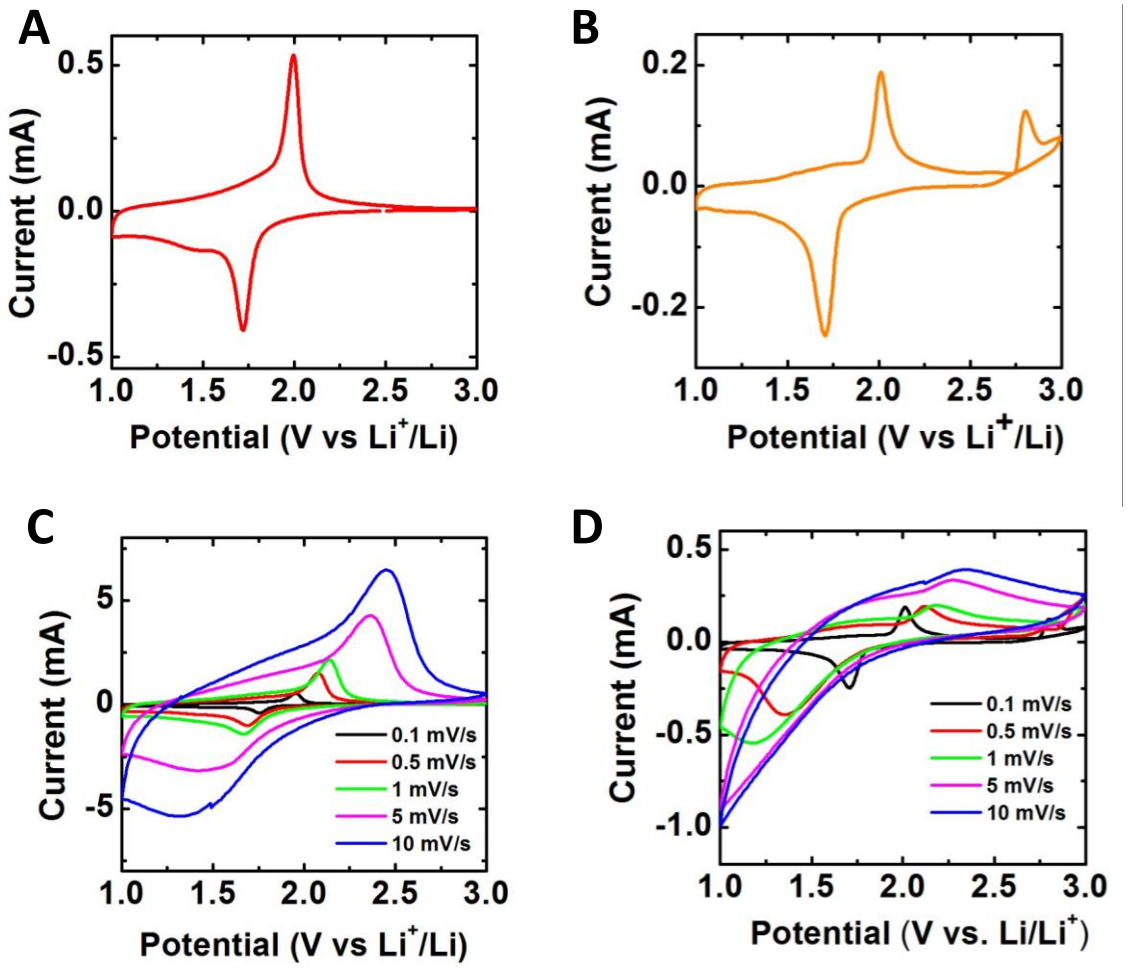

Figure 7. Electrochemical performance of the PT-TiO_2 and P25 TiO_2 in a half-cell LIB. Cyclic voltammogram of (A) PT-TiO_2 and (B) P25 TiO_2 at 0.1 mV s^{-1}. Cyclic voltammograms of (C) PT-TiO_2 and (D) P25 TiO_2 at 0.1, 0.5, 1, 5 and 10 mV s^{-1}.

The 1st, 2sd, 10th and 50th charged/discharged curves at 0.1 C of the P25 and synthesized nanocomposite are shown in Figure 8A and 8B, respectively. Significantly, three characteristic regions can be observed in the discharged branches: the monotonous voltage drop region to 1.78V in which the insertion of lithium ion is very poor, the plateau voltage region of approximately 1.75-1.80V which can be linked to the equilibrium between tetragonal and orthorhombic phase with reversible lithium insertion/extraction reaction and the larger potential slope from 1.73V to 1V where the lithium insertion processes are favoured by the electric field forces.[32] The specific capacities and coulombic efficiencies of both anode materials were investigated at 0.1 C over 100 cycles to get insights on the charge/discharge electrochemical properties of both TiO_2-based anode materials (Figure 8C). The initial charge/discharge capacities for the PT-TiO_2 and P25 are 228 mA h g^{-1} and 163 m A g^{-1}, and 215 mA h g^{-1} and 168 m A g^{-1}, respectively, giving rise to coulombic efficiencies around 79% and 74%, respectively. The low coulombic efficiency values could be interpreted by the irreversible accumulation of lithium anions inside TiO_2 crystalline network and the subsequent formation of a partial solid electrolyte interphase (SEI) layer. Afterwards, in the second cycle, the charge/discharge capacities decrease to 161 mA h g^{-1} and 151 m A g^{-1} for the nanocomposite and to 142 mA g h^{-1} and 137 mA h g^{-1} for the commercial TiO_2, while the coulombic efficiencies rise up to 100% and 93%, respectively. However, after 100 cycles, the discharges capacities drop off to 109 mA g h^{-1} (76% of capacity retention of the second cycle) for the nanocomposite and 28 mA g h^{-1} (20% of capacity retention regarding to the second cycle) for the commercial TiO_2 LIBs, indicating the superior performance of the nanohybrid anode materials.

We have to highlight that the PT-TiO_2 anode nanomaterials delivered a reversible capacity of 107 mA h g^{-1} at 0.1C, which is in the order of other TiO_2 based electrode materials.[35,36]

The rate capabilities at 0.1 C, 0.2 C, 0.5 C, 1 C and 2C were performed to compare the electrochemical performance of both batteries at different current densities (Figure 8D). As it is expected, the capacity of the commercial TiO_2 decrease rapidly at higher rate cycling values. P25 anodes deliver capacities of 145 mA g h^{-1}, 97 mA g h^{-1}, 25 mA g h^{-1}, 11 mA g h^{-1} and 5 mA g h^{-1} at 0.1 C, 0.2 C, 0.5C, 1C and 2C, respectively. On the other hand, PT-TiO_2 nanocomposites exhibit higher capacities of 167 mA g h^{-1}, 140 mA g h^{-1}, 116 mA g h^{-1}, 98 mA h g^{-1} and 84 mA g h^{-1}, respectively, demonstrating the remarkable effect of structural TiO_2 changes produced by the biotemplated approach on the electrochemical performances of the PT-TiO_2 nanocomposite anode electrodes. Notably, lower crystallinity features of the nanocomposite materials could create a number of structural defects in the crystalline TiO_2 networks which allow the transport of Li ions across the defects and in turn the improvements of their performances as anode electrodes. In brief, the obtained capacities values of the PT-TiO_2 nanomaterial are very close to the values reported for high-performance LIBs based on carbon coated hollow TiO_2 microspheres, which represent, up to now, in terms of specific capacity, retention and coulombic efficiency, one of the more successful TiO_2 based lithium ion batteries.[37,38]

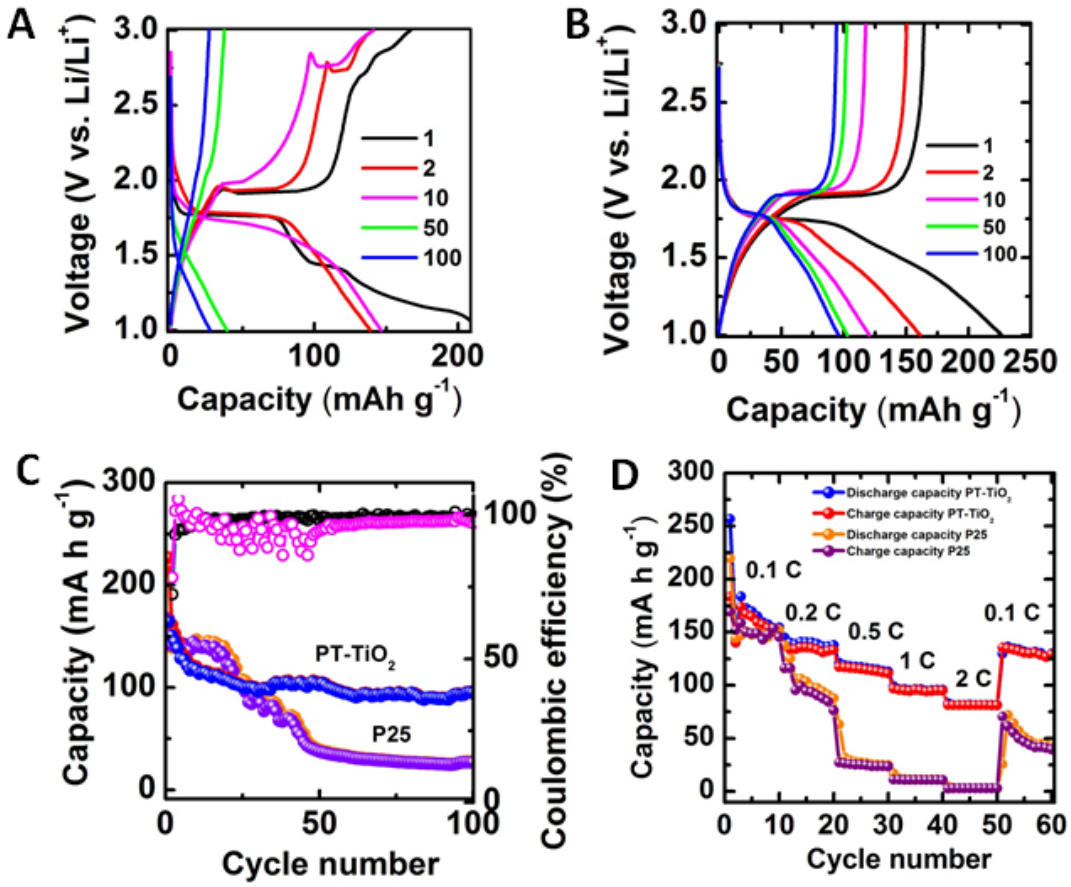

Figure 8. Charge-discharge profiles for (A) P25 TiO_2 and (B) PT-TiO_2 at a current rate of 0.1 A g^{-1} (approximate to 0.3C). (C) Specific capacity and coulombic efficiency versus cycle number for PT-TiO_2 and P25 TiO_2 materials, respectively, at 0.1 A g^{-1} and (D) Rate capability performances of both anode materials at different current densities from 0.1 C to 2C, returning to 0.1 C for PT-TiO_2 and P25, respectively. (1C = 335 $mAhg^{-1}$)

Conclusions

Valorisation of egg white from expired eggs was accomplished through their use as template in the synthesis of titania with upgraded morphological properties. Surface area increased from 10 to 139 m^2 g^{-1} by employing egg white as template. Remarkably the synthetic process was carried out

by a water-free (or any solvent) mechanochemical strategy. The obtained composite material presented a homogenous particles size distribution, with a mean radius of 5.2 nm. PT-TiO_2 demonstrated to be a good candidate for their use in catalytic and energy storage applications. Controllable and selective oxidation of diphenyl sulfide was achieved employing PT-TiO_2 as catalytic material. In addition, the synthesized nanocomposite has demonstrated to be a successful candidate for the design of highly sustainable LIBs batteries. The template approach enables a notable improvement on the TiO_2 surfaces properties which in turn boost the Li ion transport across the crystalline semiconductor network and the electrochemical performances of the resulting LIBs.

Acknowledgements

Rafael Luque gratefully acknowledges MINECO for funding project CTQ2016-78289-P, co-financed with FEDER funds. Daily Rodriguez-Padron also gratefully acknowledges MINECO for providing a research contract under the same project. Alain R. Puente-Santiago acknowledges the Research Program of the University of Cordoba for its financial support through a postdoctoral contract (Modality 5.1). M. J. Muñoz-Batista acknowledges MINECO for a Juan de la Cierva postdoctoral contract (Ref. FJCI-2016-29014). RUDN University Program 5-100 has contributed to the preparation of this work.

References

(1) Palo, D. R.; Dagle, R. A.; Holladay, J. D. Methanol Steam Reforming for Hydrogen Production. *Chem. Rev.* **2007**, *107*, 3992–4021, DOI: 10.1021/CR050198B.

(2) Chu, S.; Cui, Y.; Liu, N. The Path towards Sustainable Energy. *Nat. Mater.* **2017**, *16* (1), 16–22, DOI: 10.1038/nmat4834.

(3) Grey, C. P.; Tarascon, J. M. Sustainability and in Situ Monitoring in Battery Development. *Nat. Mater.* **2017**, *16* (1), 45–56, DOI: 10.1038/nmat4777.

(4) Rodriguez-Padron, D.; Puente-Santiago, A.; Balu, A. M.; Munoz-Batista, M. J.; Luque, R. Environmental Catalysis: Present and Future. *ChemCatChem* **2018**, *10*, DOI: 10.1002/cctc.201801248.

(5) Muñoz Batista, M. J.; Rodríguez-Padrón, D.; Puente Santiago, A. R.; Luque, R. Mechanochemistry: Towards Sustainable Design of Advanced Nanomaterials for Electrochemical Energy Storage and Catalytic Applications. *ACS Sustain. Chem. Eng.* **2018**, *6* (8), 9530–9544, DOI: 10.1021/acssuschemeng.8b01716.

(6) Colmenares, J. C.; Luque, R. Heterogeneous Photocatalytic Nanomaterials: Prospects and Challenges in Selective Transformations of Biomass-Derived Compounds. *Chem. Soc. Rev.* **2014**, *43* (3), 765–778, DOI: 10.1039/C3CS60262A.

(7) Kubacka, A.; Fernández-García, M.; Colón, G. Advanced Nanoarchitectures for Solar Photocatalytic Applications. *Chem. Rev.* **2012**, *112* (3), 1555–1614, DOI: 10.1021/cr100454n.

(8) Varma, R. S. Journey on Greener Pathways: From the Use of Alternate Energy Inputs and Benign Reaction Media to Sustainable Applications of Nano-Catalysts in Synthesis and Environmental Remediation. *Green Chem.* **2014**, *16* (4), 2027, DOI: 10.1039/c3gc42640h.

(9) Lops, C.; Ancona, A.; Di Cesare, K.; Dumontel, B.; Garino, N.; Canavese, G.; Hérnandez, S.; Cauda, V. Sonophotocatalytic Degradation Mechanisms of Rhodamine B Dye via Radicals Generation by Micro- and Nano-Particles of ZnO. *Appl. Catal. B Environ.* **2019**, *243*, 629–640, DOI: 10.1016/J.APCATB.2018.10.078.

(10) Zuliani, A.; Munoz-Batista, M. J.; Luque, R. Microwave-Assisted Valorization of Pig Bristles: Towards Visible Light Photocatalytic Chalcocite Composites. *Green Chem.* **2018**, *20*, 3001–3007, DOI: 10.1039/C8GC00669E.

(11) Li, W.; Wang, F.; Liu, Y.; Wang, J.; Yang, J.; Zhang, L.; Elzatahry, A. A.; Al-Dahyan, D.; Xia, Y.; Zhao, D. General Strategy to Synthesize Uniform Mesoporous TiO2/Graphene/Mesoporous TiO2 Sandwich-Like Nanosheets for Highly Reversible Lithium Storage. *Nano Lett.* **2015**, *15* (3), 2186–2193, DOI: 10.1021/acs.nanolett.5b00291.

(12) Lee, D.-H.; Lee, B.-H.; Sinha, A. K.; Park, J.-H.; Kim, M.-S.; Park, J.; Shin, H.; Lee, K.-S.; Sung, Y.-E.; Hyeon, T. Engineering Titanium Dioxide Nanostructures for Enhanced Lithium-Ion Storage. J. Am. Chem. Soc. **2018**, 140 (48), 16676–16684, DOI: 10.1021/jacs.8b09487.

(13) Linsebigler, A. L.; Lu, G.; Yates, J. T. Photocatalysis on TiO2 Surfaces: Principles, Mechanisms, and Selected Results. *Chem. Rev.* **1995**, *95* (3), 735–758, DOI: 10.1021/cr00035a013.

(14) Henderson, M. A. A Surface Science Perspective on TiO2 Photocatalysis. *Surf. Sci. Rep.* **2011**, *66* (6–7), 185–297, DOI: 10.1016/J.SURFREP.2011.01.001.

(15) Roy, P.; Berger, S.; Schmuki, P. TiO2 Nanotubes: Synthesis and Applications. *Angew. Chem. Int. Ed. Engl.* **2011**, *50* (13), 2904–2939. https://doi.org/10.1002/anie.201001374.

(16) Dahl, M.; Liu, Y.; Yin, Y. Composite Titanium Dioxide Nanomaterials. *Chem. Rev.* **2014**, *114* (19), 9853–9889, DOI: 10.1021/cr400634p.

(17) Chen, X.; Mao, S. S. Titanium Dioxide Nanomaterials: Synthesis, Properties, Modifications, and Applications. *Chem. Rev.* **2007**, *107* (7), 2891–2959, DOI: 10.1021/cr0500535.

(18) Mattsson, A.; Leideborg, M.; Larsson, K.; Westing, G.; Österlund, L. Adsorption and Solar Light Decomposition of Acetone on Anatase TiO 2 and Niobium Doped TiO2 Thin Films. *J. Phys. Chem. B* **2006**, *110* (3), 1210–1220, DOI: 10.1021/jp055656z.

(19) Soria, J.; Sanz, J.; Sobrados, I.; Coronado, J. M.; Herna, M. D.; Fresno, F. Water-Hydroxyl Interactions on Small Anatase Nanoparticles Prepared by the Hydrothermal Route. *J. Phys. Chem. C* **2010**, *114*, 16534–16540, DOI: 10.1021/jp105131w.

(20) Muñoz-Batista, M. J.; Nasalevich, M. A.; Savenije, T. J.; Kapteijn, F.; Gascon, J.; Kubacka, A.; Fernández-García, M. Enhancing Promoting Effects in G-C3N4-Mn+/CeO2-TiO2 Ternary Composites: Photo-Handling of Charge Carriers. *Appl. Catal. B Environ.* **2015**, *176–177*, 687–698, DOI: 10.1016/j.apcatb.2015.04.051.

(21) Caudillo-Flores, U.; Muñoz-Batista, M. J.; Kubacka, A.; Zárate-Medina, J.; Cortés, J. A.; Fernández-García, M. Measuring and Interpreting Quantum Efficiency of Acid Blue 9 Photodegradation Using TiO2-Based Catalysts. *Appl. Catal. A Gen.* **2018**, *550* (July 2017), 38–47, DOI: 10.1016/j.apcata.2017.10.016.

(22) Muñoz-Batista, M. J.; Caudillo-Flores, U.; Ung-Medina, F.; del Carmen Chávez-Parga, M.; Cortés, J. A.; Kubacka, A.; Fernández-García, M. Gas Phase 2-Propanol Degradation Using Titania Photocatalysts: Study of the Quantum Efficiency. *Appl. Catal. B Environ.* **2017**, *201*, 400–410, DOI: 10.1016/j.apcatb.2016.08.014.

(23) Agency, U. S. E. P. Sustainable Management of Food https://www.epa.gov/sustainable-management-food (accessed Nov 30, 2018).

(24) Gao, S.; Yan, Y.; Chen, G. External Water-Free Approach toward TiO2Nanoparticles Embedded in Biomass-Derived Nitrogen-Doped Carbon. *ACS Sustain. Chem. Eng.* **2016**, *4* (3), 844–850, DOI: 10.1021/acssuschemeng.5b00904.

(25) Yan, J.; Wu, G.; Li, L.; Yu, A.; Sun, X.; Guan, N. Synthesis of Uniform TiO2 Nanoparticles with Egg Albumen Proteins as Novel Biotemplate. *J. Nanosci. Nanotechnol.* **2010**, *10* (9), 5767–5775, DOI: 10.1166/jnn.2010.2501.

(26) Liu, R.-L.; Ji, W.-J.; He, T.; Zhang, Z.-Q.; Zhang, J.; Dang, F.-Q. Fabrication of Nitrogen-Doped Hierarchically Porous Carbons through a Hybrid Dual-Template Route for CO2 Capture and Haemoperfusion. *Carbon N. Y.* **2014**, *76*, 84–95, DOI: 10.1016/J.CARBON.2014.04.052.

(27) Luna-Lama, F.; Rodríguez-Padrón, D.; Puente-Santiago, A. R.; Muñoz-Batista, M. J.; Caballero, A.; Balu, A. M.; Romero, A. A.; Luque, R. Non-Porous Carbonaceous Materials Derived from Coffee Waste Grounds as Highly Sustainable Anodes for Lithium-Ion Batteries. *J. Clean. Prod.* **2019**, *207*, 411–417, DOI: 10.1016/J.JCLEPRO.2018.10.024.

(28) Muñoz-Batista, M. J.; Ballari, M. M.; Cassano, A. E.; Alfano, O. M.; Kubacka, A.; Fernández-García, M. Ceria Promotion of Acetaldehyde Photo-Oxidation in a TiO2-Based Catalyst: A Spectroscopic and Kinetic Study. *Catal. Sci. Technol.* **2014**, *5* (3), 1521–1531, DOI: 10.1039/C4CY01293C.

(29) Verma, S.; Baig, R. B. N.; Nadagouda, M. N.; Varma, R. S. Sustainable Strategy Utilizing Biomass: Visible-Light-Mediated Synthesis of γ-Valerolactone. *ChemCatChem* **2016**, *8* (4), 690–693, DOI: 10.1002/cctc.201501352.

(30) Rodríguez-Padrón, D.; Puente-Santiago, A. R.; Caballero, A.; Balu, A. M.; Romero, A. A.; Luque, R. Highly Efficient Direct Oxygen Electro-Reduction by Partially Unfolded Laccases Immobilized on Waste-Derived Magnetically Separable Nanoparticles. *Nanoscale* **2018**, *10* (8), 3961–3968, DOI: 10.1039/C8NR00512E.

(31) Ouyang, W.; Muñoz-Batista, M. J.; Kubacka, A.; Luque, R.; Fernández-García, M. Enhancing Photocatalytic Performance of TiO2 in H 2 Evolution via Ru Co-Catalyst Deposition. *Appl. Catal. B Environ.* **2018**, *238*, 434–443, DOI: 10.1016/j.apcatb.2018.07.046.

(32) Gao, S.; Yan, Y.; Chen, G. External Water-Free Approach toward TiO2 Nanoparticles Embedded in Biomass-Derived Nitrogen-Doped Carbon. *ACS Sustain. Chem. Eng.* **2016**, *4* (3), 844–850, DOI: 10.1021/acssuschemeng.5b00904.

(33) Radko, M.; Kowalczyk, A.; Bidzińska, E.; Witkowski, S.; Górecka, S.; Wierzbicki, D.; Pamin, K.; Chmielarz, L. Titanium Dioxide Doped with Vanadium as Effective Catalyst for Selective Oxidation of Diphenyl Sulfide to Diphenyl Sulfonate. *J. Therm. Anal. Calorim.* **2018**, *132* (3), 1471–1480, DOI: 10.1007/s10973-018-7119-9.

(34) Al-Maksoud, W.; Daniele, S.; Sorokin, A. B. Practical Oxidation of Sulfides to Sulfones by H2O2catalysed by Titanium Catalyst. *Green Chem.* **2008**, *10* (4), 447–451, DOI: 10.1039/b717696a.

(35) Ren, M.; Xu, H.; Li, F.; Liu, W.; Gao, C.; Su, L.; Li, G.; Hei, J. Sugarapple-like N-Doped TiO2@carbon Core-Shell Spheres as High-Rate and Long-Life Anode Materials for Lithium-Ion Batteries. *J. Power Sources* **2017**, *353*, 237–244, DOI: 10.1016/J.JPOWSOUR.2017.04.015.

(36) Senthil, C.; Kesavan, T.; Bhaumik, A.; Yoshio, M.; Sasidharan, M. Nitrogen Rich Carbon Coated TiO2 Nanoparticles as Anode for High Performance Lithium-Ion Battery. *Electrochim. Acta* **2017**, *255*, 417–427, DOI: 10.1016/J.ELECTACTA.2017.10.001.

(37) Jin, Z.; Yang, M.; Wang, J.; Gao, H.; Lu, Y.; Wang, G. One-Pot Fabrication of Hierarchical Nanosheet-Based TiO2-Carbon Hollow Microspheres for Anode Materials of High-Rate Lithium-Ion Batteries. *Chem. - A Eur. J.* **2016**, *22* (17), 6031–6036, DOI: 10.1002/chem.201505099.

(38) Liu, H.; Li, W.; Shen, D.; Zhao, D.; Wang, G. Graphitic Carbon Conformal Coating of Mesoporous TiO2 Hollow Spheres for High-Performance Lithium Ion Battery Anodes. *J.*

Am. Chem. Soc. **2015**, *137* (40), 13161–13166, DOI: 10.1021/jacs.5b08743.

Table of Contents (TOC GRAPHIC)

Protein-templated titania nanomaterial with remarkable textural properties for catalysis and LIBs devices.